SIO2331 Electrical Methods in Geophysics

Lecture 8: The Two-Dimensional MT Forward Problems

Notes from Bob Parker, 2007

Introduction

In Lecture 7 we saw how to solve the forward problem associated with the three most common electrical sounding methods for one-dimensional conductivity structures. In each case the results would be expressed compactly in either analytic form, or at least in a very simple computer code. We now progress to two-dimensional systems, where we find a less satisfactory state of affairs. Things do simplify, but there are essentially no nontrivial analytic solutions. As described already in Lecture 6, the general electromagnetic induction problem in two-dimensions can be decomposed into two independent modes, the Transverse Magnetic (TM) and the Transverse Electric (TE) modes. We shall see how to write the differential equations for these two modes, which are different, and their corresponding boundary conditions.

Transverse Magnetic Mode Induction

For all two-dimensional systems, the conductivity is a function of x and z only: $\sigma = \sigma(x, z)$; the y directions is taken to be the strike of the local geology. In the TM mode the magnetic field is parallel to the strike, so we can $\mathbf{B} = \hat{\mathbf{y}} B(x, z) e^{i\omega t}$, where $B(x, z)$ is a complex scalar function. We assert that everything is invariant in the y direction, or $\partial/\partial y = 0$, which leads to the picture, illustrated below, that the currents and electric field have no y component—they flow in the x-y plane. Let us remind ourselves of two of the pre-Maxwell equations:

$$\nabla \times \mathbf{B} = \mu_0 \mathbf{J} \tag{1}$$

$$\nabla \times \mathbf{E} = -i\omega \mathbf{B}. \tag{2}$$

We need to relate current density to electric field via Ohm's law:

$$\mathbf{J} = \sigma \mathbf{E}. \tag{3}$$

In the TM problem we usually eliminate **E**. Recall (8) from Lecture 3,

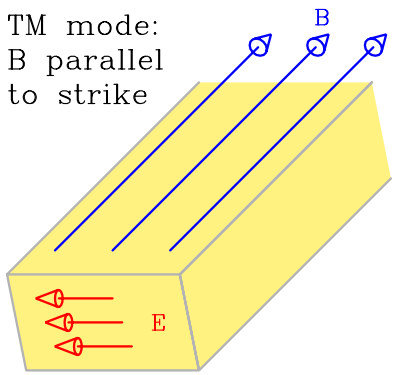

obtained by simply combining the curl of (1) with (2) and (3):

$$\nabla \times \left[\frac{1}{\mu_0 \sigma} \nabla \times \mathbf{B} \right] = -i\omega \mathbf{B} . \tag{4}$$

Introducing the material resistivity $\rho = 1/\sigma$ for convenience, we have

$$\nabla \times (\rho \nabla \times \mathbf{B}) = -i\omega\mu_0 \mathbf{B} . \tag{5}$$

We now insert $\mathbf{B} = \hat{\mathbf{y}} B$, the fact that $\mathbf{B}$ points in the y direction:

$$-i\omega\mu_0 \hat{\mathbf{y}} B = \nabla \times [\rho \nabla \times (\hat{\mathbf{y}} B)] = \nabla \times [\rho \nabla B \times \hat{\mathbf{y}}] \tag{6}$$

$$= \rho \nabla B \nabla \cdot \hat{\mathbf{y}} - \hat{\mathbf{y}} \nabla \cdot (\rho B) + (\hat{\mathbf{y}} \cdot \nabla)(\rho \nabla B) - (\rho \nabla B \cdot \nabla)\hat{\mathbf{y}} \tag{7}$$

We have used the vector identities for $\nabla \times (s\mathbf{A})$ and $\nabla \times (\mathbf{A} \times \mathbf{B})$. In (7) the first and third terms vanish because $\hat{\mathbf{y}}$ is constant and the third is zero because $\hat{\mathbf{y}} \cdot \nabla = \partial/\partial y = 0$. Thus one term survives in (7) and (6) reduces to

$$\nabla \cdot (\rho \nabla B) = i\omega\mu_0 B \tag{8}$$

where the grad operator may be read as the 2-D version. This is the deceptively simple equation for the scalar B in the TM mode. Notice that we did not show the divergence of $\mathbf{E}$ vanishes here, and indeed it does not do so in general: charges may accumulate on interfaces, and so we cannot assume continuity of $\mathbf{E}$ normal to surfaces.

Boundary conditions are needed for B. It is common to solve the induction problem in a layer of finite thickness, $0 \le z \le H$. Suppose a perfect conductor ($\sigma = \infty$) at the depth $z = H$. Then from Ohm's law $\mathbf{E}$ vanishes there, just outside the region. Because $\mathbf{E}$ parallel to the base is continuous, we conclude that $E_x = 0$ in the regular conductor, and from the x component of (1) this becomes the boundary condition for B:

$$\frac{\partial B}{\partial z} = 0, \quad \text{on } z = H . \tag{9}$$

Equation (9) is called a **Neumann boundary condition** which is the name for conditions that specify a normal derivative. At the Earth's surface there is an insulator, so that $J_z = 0$, no current flows vertically. The z component of (1) then gives us $\partial B/\partial x = 0$, which we can integrate horizontally to give the surface boundary condition:

$$B = B_0 = \text{constant}, \quad \text{on } z = 0 . \tag{10}$$

This is an example of a **Dirichlet boundary condition**, where the value of the solution is specified. So in the TM mode the currents $\mathbf{J}$ within the body do not generate magnetic fields above the conductor, and the source field is observed at the surface; in other words, the induced magnetic fields within the conductor do not leak out into the space above—they are *toroidal fields* (see Lecture 3). If an insulator were placed at the bottom as well as the top of the system, we would find two Dirichlet conditions; it is an exercise for the student to decide what value the constant should be at $z = H$. What to do about the sides? We can place perfect conductors or insulators at a finite distance. More

commonly one assumes the conductivity tends to a constant value as $|x| \to \infty$, and then the solution can be forced to be that for a finite layer as derived in Lecture 7.

For comparison with observation we need the Z_{xy} element of the impedance tensor, or

$$Z_{xy} = \frac{E_x}{B_y} = -\frac{1}{\mu_0 \sigma B} \frac{\partial B}{\partial z} \tag{11}$$

evaluated at the observation sites on $z = 0$ at a variety of frequencies ω. Of course this means solving (8) subject to the appropriate boundary conditions for each of the frequencies of interest.

Transverse Electric Mode Induction

The TE mode orients the driving **B** field orthogonal to the geologic strike, and therefore the source is $\mathbf{B} = \hat{\mathbf{x}} B_0 e^{i\omega t}$. But just as in the previous section everything remains constant as we move in the y direction, so again $\partial/\partial y = 0$. The electric field and the currents all flow in the y direction as pictured below. So we write $\mathbf{E} = \hat{\mathbf{y}} E(x,z) e^{i\omega t}$ with the complex scalar function $E(x,z)$. From (1) we see

$$0 = \nabla \cdot \mathbf{J} = \nabla \cdot (\sigma \mathbf{E}) = \sigma \nabla \cdot \mathbf{E} + \mathbf{E} \cdot \nabla \sigma . \tag{12}$$

Since **E** points along y and $\nabla\sigma$ lies in the x-z plane, the dot product in (12) vanishes and we conclude for the TE mode that

$$\nabla \cdot \mathbf{E} = 0 . \tag{13}$$

Hence the vector **E** is continuous at interfaces, not just the tangential components.

Recall from Lecture 3 we derived a general equation for the electric field in the pre-Maxwell approximation:

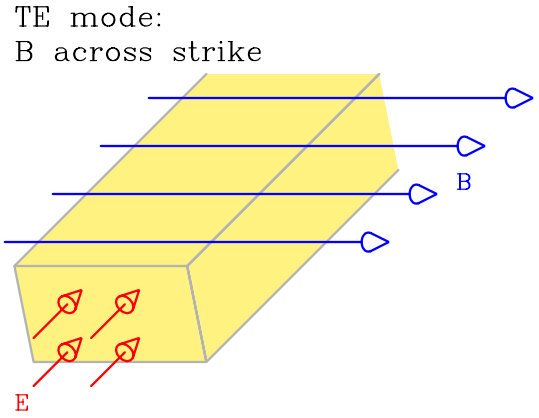

$$\nabla^2\mathbf{E} - \nabla(\nabla\cdot\mathbf{E}) = i\omega\mu_0\sigma\mathbf{E}. \tag{14}$$

Recognizing (13), and setting $\mathbf{E} = \hat{\mathbf{y}}\,E(x,z)e^{iot}$ we get the differential equation for the complex electric field scalar:

$$\nabla^2 E = i\omega\mu_0\sigma E \tag{15}$$

essentially the same equation that we found for induction in a uniform halfspace, but here σ varies in the x-z plane, not with z alone.

Again we need boundary conditions, which turn out to be surprisingly awkward for the TE case. Let us put an infinitely conducting base at $z = H$. Now because all components of $\mathbf{E}$ are continuous at interfaces, this translates simply into

$$E = 0, \quad \text{on } z = H. \tag{16}$$

That was the easy part. The fact that, due to the insulator, there is no vertical current at $z = 0$ has no force, since $E_z = \sigma\mathbf{J}_z = 0$ automatically for all TE solutions. We have to assert two things at $z = 0$; first there is an insulator in $z < 0$; second the driving $\mathbf{B}$ is uniform and in the x direction. In the TM mode we showed through the boundary condition that the induced magnetic fields within the conductor are toroidal. Here the internally generated magnetic fields do penetrate into the insulator and so we must write the magnetic field just above $z = 0$ as

$$\mathbf{B} = \hat{\mathbf{x}}B_0 + \mathbf{B}^J \tag{17}$$

where $\mathbf{B}^J$ is the magnetic field due to the currents $\mathbf{J}$. We need to assert the condition that this field comes from sources within, which could be done by writing an integral over the $\mathbf{J}$, although that would be incredibly inefficient computationally, and it would not exactly constitute a *boundary condition*. Instead, we appeal to potential theory in two dimensions. Above the conductor no currents flow, so by the same theory used for Lecture 3, (32)-(33) we have

$$\mathbf{B} = -\nabla\Omega; \quad \nabla^2\Omega = 0. \tag{18}$$

This is how we put the presence of an insulator into the boundary condition. Next take the x component of (17) on $z = 0$:

$$B_x = B_0 + B_x^J. \tag{19}$$

But this is a 2-D system; then the x and z components of a harmonic field with sources below ground are related via a **Hilbert transform**:

$$B_x^J(x,0) = \frac{1}{\pi}\int_{-\infty}^{\infty} \frac{B_z^J(\xi,0)}{x-\xi}\,d\xi. \tag{20}$$

See Chapter 12, Blakely, R. J., *Potential Theory in Gravity and Magnetic Applications*, Cambridge University Press, New York, 1995. We insert (20) into (19), and use (2) to obtain:

$$\frac{\partial E}{\partial z} + \frac{1}{\pi}\int_{-\infty}^{\infty} \frac{\partial E/\partial x}{x-\xi}\, d\xi = i\omega B_0, \quad \text{on } z = 0 \tag{21}$$

which is the proper top-surface boundary condition for TE mode induction.

Equation (21) is not an easy condition to apply, particularly numerically. So instead for numerical models a kludge is adopted: the insulating layer above the ground is included in the numerical model, and at some height above the system the approximate condition that $\mathbf{B} = \hat{\mathbf{x}} B_0$ is applied; here the approximation being made is that the internal fields $\mathbf{B}^J$ have died away to negligible values at the top of the insulating layer.

Once more we use the model to predict measured values at the surface of the appropriate component in the impedance tensor:

$$Z_{yx} = \frac{E_y}{B_x} = \frac{E}{i\omega\, \partial E/\partial z}, \quad \text{on } z = 0. \tag{24}$$

SIO 231 Electrical Methods in Geophysics

Lecture 12: Numerical Methods for 2D and 3D EM

Guest lecture by Kerry Key, 5 November 2013

Introduction

Numerical methods for 2D and 3D modeling of EM geophysical techniques rely on approaches that break up the heterogeneous model domain into finite cells of piecewise constant conductivity. With a grid defined and a suitable choice of boundary conditions that describe the particular EM problem at hand, the solutions to Maxwell's equations can be found by one of several well-studied numerical methods. The majority of practical EM modeling codes in use today rely on the finite difference (FD) and finite element (FE) methods. Other useful approaches include the integral equation (IE) method and the finite volume (FV) method, but these are used less frequently so we won't spend much time discussing them. All of these methods rely on numerical approximations to the governing differential equations, hence we will start our journey with a review of Maxwell's equations. We will consider frequency domain electromagnetic induction in heterogeneous, isotropic conducting media $\sigma = \sigma(x, y, z)$. We will assume that magnetic permeability variations are negligible so $\mu = \mu_0$. We will assume that the angular frequency ω is low enough and the conductivity σ is large enough such that the quasi-static approximation holds:

$$\sigma \gg \omega\epsilon, \tag{1}$$

where ϵ is the dielectric permittivity. When this relation holds, we can safely neglect the electric displacement current $\mathbf{D}$ in Ampere's law. Maxwell's equations are then

$$\begin{aligned}
\nabla \times \mathbf{E} &= -i\omega\mu_0\mathbf{H} - i\omega\mathbf{M}_s, && (2)\\
\nabla \times \mathbf{H} &= \sigma\mathbf{E} + \mathbf{J}_s, && (3)\\
\nabla \cdot \mathbf{B} &= 0, && (4)\\
\nabla \cdot \mathbf{E} &= \rho_e/\epsilon, && (5)
\end{aligned}$$

where $\mathbf{J}_s$ and $\mathbf{M}_s$ are time varying electric and magnetic sources and ρ_e is electric charge density. For a given EM geophysical technique, only one source type is typically used at a time, but for generality we will simultaneously include both electric

and magnetic sources in our derivations. For example in the MT method the EM fields are generated by a sheet of current in the ionosphere that diffuses down into the Earth, hence only the source $\mathbf{J}_s$ is needed[1]. For active source EM methods that rely on a transmitter to generate the EM field, the source terms correspond to electric or magnetic transmitters that are non-zero only at the source location(s). For point dipole transmitters, $\mathbf{J}_s$ and $\mathbf{M}_s$ can be represented as vector Dirac delta functions located at the sources. Finite length sources such as long wires and rectangular loops can be modeled by representing $\mathbf{J}_s$ as a line or sequence of line segments.

One approach to numerically modeling Maxwell's equations is to directly discretize equations 2 and 3 on a numerical grid. However, that means there are six unknowns to solve for, given the three vector components of each of $\mathbf{E}$ and $\mathbf{H}$. Instead, these equations can be decoupled by rewriting equation 2 for $\mathbf{H}$ and inserting this into equation 3 , yielding

$$\nabla \times \nabla \times \mathbf{E} + i\omega\mu_0\sigma\mathbf{E} = -i\omega\mu_0\mathbf{J}_s - i\omega\nabla \times \mathbf{M}_s. \tag{6}$$

Similarly, rewriting equation 3 for $\mathbf{E}$ and inserting this into equation 2 yields the uncoupled equation for $\mathbf{H}$

$$\nabla \times \frac{1}{\sigma}\nabla \times \mathbf{H} + i\omega\mu_0\mathbf{H} = \nabla \times \frac{\mathbf{J}_s}{\sigma} - i\omega\mathbf{M}_s. \tag{7}$$

Note that since the conductivity can vary spatially $\sigma = \sigma(x, y, z)$, it must remain inside the derivative operators for now. Equations 6 and 7 are sometimes referred to as the *curl-curl* equations in the EM geophysics community. They describe the 3D vector electric and magnetic fields produced from the imposed sources $\mathbf{J}_s$ and $\mathbf{M}_s$ and have only three unknowns each. The right hand side of equation 6 shows that electric fields are produced by both electric current sources (one would hope so) and also the curl of a magnetic source. Examining the right hand side of equation 7, we see that magnetic fields are produced by magnetic sources and the curl of any electric current sources present.

For general 3D problems, equations 6 and 7 could be solved separately to give the complete $\mathbf{E}$ and $\mathbf{H}$ fields. However, 3D models can be extremely large (several million unknowns or more are required for realistic problems) and the solution of either equation often requires a significantly long computational run-time. Thus, it is common to solve only one of the equations and then to use a numerical approximation

[1]For MT modeling $\mathbf{J}_s$ is a laterally uniform sheet of current at around 100 km altitude above the Earth's surface. However, most numerical methods instead impose the source via boundary conditions and hence set $\mathbf{J}_s = 0$ everywhere, as we will see in a later section.

to either Faraday's law or Ampere's law to find the other field. Because the $1/\sigma$ operator in equation 7 is more complicated to implement numerically, it is common to solve equation 6 for $\mathbf{E}$, and then to use equation 2 to compute $\mathbf{H}$ using a numerical approximation for the derivates of $\mathbf{E}$. However, there are other numerical considerations that can make the $\mathbf{H}$ equation more attractive for certain problems, but we don't have space to review them here.

As we will see later on, the FD and FE numerical formulations for equations 6 and 7 (and their 2D counterparts) are cast into the linear system

$$\mathbf{A}\mathbf{x} = \mathbf{b}, \tag{8}$$

$\mathbf{A}$ is a sparse complex symmetric matrix of the numerical approximation of the operators applied to the fields, $\mathbf{x}$ is a vector of unknown values of $\mathbf{E}$ or $\mathbf{H}$ and $\mathbf{b}$ is a vector containing the sourcing terms on the right hand side of equations 6 and 7. It can help to think of the linear system as simply

$$\begin{aligned} [\nabla \times \nabla \times \ + i\omega\mu_0\sigma \ ]\,[\mathbf{E}] &= [-i\omega\mu_0\mathbf{J}_s - i\omega\nabla \times \mathbf{M}_s]\,, & (9)\\ \mathbf{A}\mathbf{x} &= \mathbf{b}. & (10) \end{aligned}$$

where the brackets imply a numerical implementation such as the FD or FE methods.

An important point to note is that the left hand side operations in matrix $\mathbf{A}$ are independent of the EM source functions contained in $\mathbf{b}$. Thus, once $\mathbf{A}$ is constructed, any EM source can be applied by changing the vector $\mathbf{b}$. This makes it easy to create a generalized 3D code that can handle various sources such as MT ionospheric currents, electric or magnetic dipole transmitters and line currents such as long wires or loops. For large 3D problems, one usually solves the linear system using an iterative conjugate gradient method such as matrix-free quasi-minimal residual (QMR), which is very memory efficient since the full matrix $\mathbf{A}$ does not have to be stored in memory. However, for 2D and small 3D problems, the inverse of $\mathbf{A}$ can be rapidly computed using sparse matrix LU factorization. If one saves the LU factors, it is easy to rapidly compute the EM fields for many sources by computing the matrix-matrix product

$$\mathbf{X} = \mathbf{A}^{-1}\mathbf{B}, \tag{11}$$

where $\mathbf{B} = [\mathbf{b}_1\,\mathbf{b}_2\,\mathbf{b}_3\ldots]$, $\mathbf{X} = [\mathbf{x}_1\,\mathbf{x}_2\,\mathbf{x}_3\ldots]$ and the subscripts refer to the transmitter source number. For methods such as marine controlled-source EM, where a transmitter is towed continuously over the seabed, this *multiple right hand side* vector technique can drastically reduce the computational time.

Scattered Field Formulations

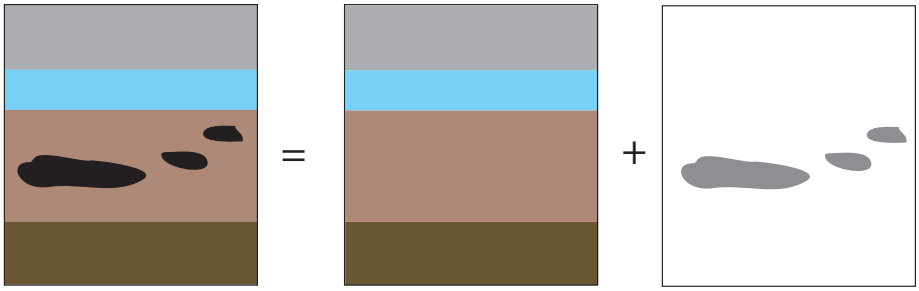

Figure 1: Decomposing a conductivity model into primary and secondary parts.

Equations 6 and 7 are known as total field equations since $\mathbf{E}$ and $\mathbf{H}$ represent the complete electric and magnetic fields. However, sometimes it is beneficial to perform a decomposition so that the numerical model grid is only needed to compute a portion of the EM field, while the other part is computed with an analytic formula. This approach is known as the *scattered field* formulation (also referred to as a secondary field formulation). The idea behind the scattered field formulation is to decompose the total electric and magnetic fields into primary and scattered components, written as

$$\mathbf{E} = \mathbf{E}' + \mathbf{E}_0, \tag{12}$$

$$\mathbf{H} = \mathbf{H}' + \mathbf{H}_0, \tag{13}$$

where $\mathbf{E}_0$ is the primary, or background electric field, and $\mathbf{E}'$ is the scattered electric field[2], and similarly for the magnetic field. The primary fields are associated with a background conductivity σ_0, which is usually a simple layered model $\sigma_0 = \sigma_0(z)$ so that analytic methods can be used for a much faster and accurate solution. The total conductivity is thus the sum of the background conductivity and a scattering conductivity σ' (Figure 1):

$$\sigma = \sigma_0 + \sigma'. \tag{14}$$

Why do this? There are two main reasons. First, it is often the case that much of the structure of the total fields can be described by the 1D primary field, and the scattered field may relatively larger only in a few spatially confined regions of the model. Thus, by recasting the partial differential equation in terms of scattered fields,

[2]Note that here the $'$ symbol denotes the scattered field, not a derivative.

the numerical grid can be much smaller since it only has to capture the behavior of the scattered field. The second and more important reason is that the source terms $\mathbf{J}_s$ and $\mathbf{M}_s$ can contain singularities at the transmitter positions and these can be extremely cumbersome to accurately model with FD and FE grids since the extreme curvature in the field near the singularity requires a very dense model grid. With a scattered field formulation, the singularity can be removed from the FD and FE systems.

Let's recast equation 6 to see how this works. First we note that the primary field obeys the equation

$$\nabla \times \nabla \times \mathbf{E}_0 + i\omega\mu_0\sigma_0\mathbf{E}_0 = -i\omega\mu_0\mathbf{J}_s - i\omega\nabla \times \mathbf{M}_s. \tag{15}$$

Then we insert the field decomposition of equation 12 into equation 6, giving

$$\nabla \times \nabla \times (\mathbf{E}' + \mathbf{E}_0) + i\omega\mu_0\sigma(\mathbf{E}' + \mathbf{E}_0) = -i\omega\mu_0\mathbf{J}_s - i\omega\nabla \times \mathbf{M}_s. \tag{16}$$

We can expand this as

$$\nabla\times\nabla\times\mathbf{E}'+i\omega\mu_0\sigma\mathbf{E}'+\nabla\times\nabla\times\mathbf{E}_0+i\omega\mu_0\sigma_0\mathbf{E}_0+i\omega\mu_0(\sigma-\sigma_0)\mathbf{E}_0 = -i\omega\mu_0\mathbf{J}_s-i\omega\nabla\times\mathbf{M}_s. \tag{17}$$

Taking note of equation 15, we arrive at the curl-curl equation for the scattered electric field

$$\nabla \times \nabla \times \mathbf{E}' + i\omega\mu_0\sigma\mathbf{E}' = -i\omega\mu_0(\sigma - \sigma_0)\mathbf{E}_0. \tag{18}$$

This equation looks very similar to equation 6, except that now the source on the right hand side is a function of the primary field times the scattering conductivity $(\sigma-\sigma_0)$, which is non-zero only where the conductivity does not match the background. Each scattering conductivity can be thought of as an EM source current for the scattered field, or in other words a scattering current source $\mathbf{J}_{scattering} = \sigma'\mathbf{E}_0$. Note that this equation no longer contains the delta functions (and singularities) from $\mathbf{J}_s$ and $\mathbf{M}_s$, provided that the background model is chosen such that $\sigma-\sigma_0 = 0$ at the transmitter location(s).

Once a scattered field solution is computed using FD or FE methods, it is added to the analytic background solution to give the total field. A similar scattered field equation can be derived for the magnetic field equation. Despite the apparent utility of the scattered field approach, many recent modeling codes just use the total field approach and some form of adaptive model grid refinement to battle the source singularities.

Finite Difference Method

You have already been introduced to the finite difference method in the 1D diffusion equation homework problem. Since Maxwell's equations are typically given in differential form (as in equations 2 and 3), it is natural to solve them by using finite differences, where the derivative terms are approximated by taking differences of field values on a uniform or non-uniform grid of points. Let's first consider the accuracy of finite differences. Suppose we have a grid of points $x_1, x_2, x_3, \ldots, x_N$ that are evenly spaced with separation h, so $x_{i+1} = x_i + h$. We also have some function $f(x)$ that we'd like to evaluate on the grid points. The Taylor's series expansion of $f(x)$ at a the location $x + h$ can be written as

$$f(x+h) = f(x) + hf'(x) + \frac{h^2}{2}f''(x) + \sum_{n=3}^{\infty} \frac{h^n}{n!} f^n(x) \tag{19}$$

One way to use the finite difference method is to evaluate forward differences, such as

$$\frac{f(x+h) - f(x)}{h} = f'(x) + O(h), \tag{20}$$

but the approximation error is to first order with h. Instead we can use a *centered* finite difference

$$\frac{f(x+h) - f(x-h)}{2h} = f'(x) + O(h^2), \tag{21}$$

to get second order accuracy with h. In practice, what works good for EM problems is to define a *staggered grid* composed of nodes (grid points) where field components are evaluated at, and a grid of half nodes in between where the derivatives are evaluated at. An example of a staggered grid in 1D is shown in Figure 2.

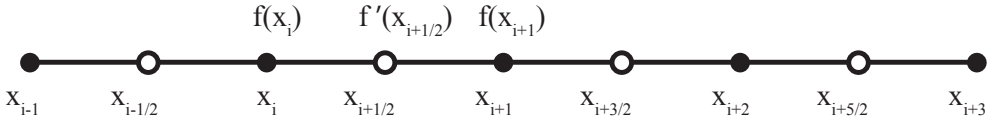

Figure 2: The 1D staggered grid for finite difference EM approximations. Function $f(x)$ is approximated at integer nodal points (black circles) and derivatives $f'(x)$ are approximated at half-nodes (white circles) using centered finite differences, giving $O(h^2)$ accuracy.

On a staggered grid, the first order derivative is approximated as

$$\frac{f(x+h)-f(x)}{h} = f'\left(x+\frac{h}{2}\right) + O(h^2). \tag{22}$$

Two first order derivatives can be combined to yield a second order derivative, such as

$$\frac{f'\left(x+\frac{h}{2}\right) - f'\left(x-\frac{h}{2}\right)}{h} = \frac{f(x+h)-2f(x)+f(x-h)}{h^2} = f''(x) + O(h^2). \tag{23}$$

Note that while the first order derivative is evaluated on the half-grid, the second order derivative is evaluated on the integer grid. This is practical for the EM problems of interest since we will have the field quantity and it's second order derivative evaluated at the same points.

2D Finite Difference Method

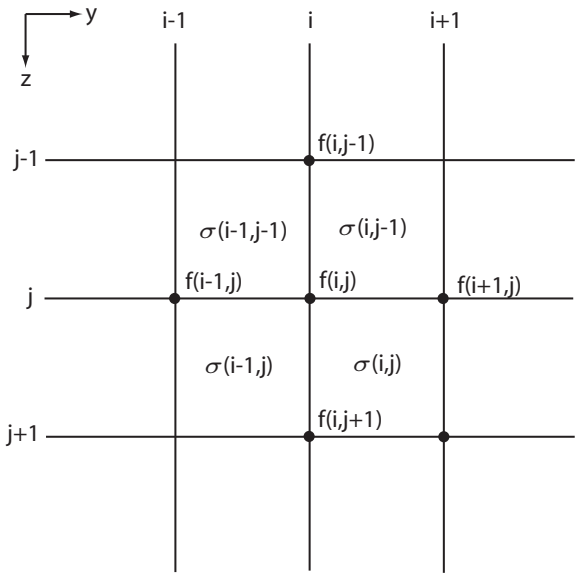

Figure 3: The 5 point stencil for the 2D finite difference method. Field values are evaluated at nodal points and conductivities are constant within rectangles between nodal points.

To demonstrate the 2D FD method, lets consider the total field TE mode magnetotelluric problem, introduced by Bob in an earlier lecture:

$$\nabla^2 E - i\omega\mu\sigma E = 0, \tag{24}$$

where $E(y, z)$ refers to the scalar electric field component pointing along the strike x of the 2D model and the conductivity varies as $\sigma = \sigma(y, z)$. Extension to the scattered field formulation is straightforward since only the right hand side needs modification. The 2D modeling domain is subdivided into a rectangular grid of conductivities with uniform grid of nodes with horizontal and vertical spacing h. Non-uniform grid spacing is possible but we won't consider than here since that formulation obscures the simplicity of the FD method. Field values will be evaluated on nodal points. The standard 2D stencil for finite differences consists of a field point and the 4 neighboring nodal points (above and below, and on the left and right), as shown in Figure 3. We evaluate the derivative terms using the second order FD approximation in equation 23. For nodal point i, j, the finite difference approximation to equation 24 is written as

$$\frac{1}{h^2}(E_{i-1,j} + E_{i+1,j} + E_{i,j-1} + E_{i,j+1} - 4E_{i,j}) - i\omega\mu\sigma E_{i,j} = 0. \tag{25}$$

Note that we have not yet assigned a conductivity σ. If the four cells surrounding node i, j have unique conductivities, we could choose from four possible conductivities. We do not have room to explore the details here, but Brewitt-Taylor and Weaver (1976) show that using $\sigma_{avg} = \frac{1}{4}(\sigma_{i-1,j-1} + \sigma_{i-1,j} + \sigma_{i,j-1} + \sigma_{i,j})$ is suitable when the contact is planar (the boundary is a vertical or horizontal plane). For the case when all four conductivities are different, there is no correct conductivity average that meets all boundary conditions, but the average conductivity is used anyway since it is the best available option. This is one weakness of the finite difference method. However, in practice the error introduced by this can be made small by creating models with only small conductivity jumps between cells or by creating a fine node spacing near larger conductivity contrasts.

We move the 5-point finite difference stencil (equation 25) over the entire grid to form the matrix system $\mathbf{Ax} = \mathbf{b}$. Here is what one row the system corresponding looks like:

$$\left[\begin{array}{ccccc} \frac{1}{h^2}, & \frac{1}{h^2}, & \frac{1}{h^2}, & \frac{1}{h^2}, & -\frac{4}{h^2} - i\omega\mu\sigma_{avg} \end{array}\right] \left[\begin{array}{c} E_{i-1,j} \\ E_{i+1,j} \\ E_{i,j-1} \\ E_{i,j+1} \\ E_{i,j} \end{array}\right] = \left[\begin{array}{c} 0 \\ 0 \\ 0 \\ 0 \\ 0 \end{array}\right]. \tag{26}$$

The specific row and column locations for each entry will depend on how the grid cells are ordered. Typically a column major ordering is used. For example, if the grid has m nodes in the vertical direction and n nodes horizontally, the first m rows of vector $\mathbf{x}$ correspond to electric fields for the nodes along the first column in the model. The next n rows will correspond to the nodes along the second column, and so forth. Since there are m by n electric field nodes, $\mathbf{A}$ is a mn by mn sparse matrix. The main diagonal of this matrix contains the terms that multiply into $E_{i,j}$ and the other form terms create two diagonals above and two diagonals below the main diagonal. Thus that matrix can easily be assembled one sparse row at time using the formula above and noting which of the five matrix diagonals the entries belong to.

Lastly we must insert boundary conditions and solve to get the electric fields at each node. For boundary conditions, we impose the Dirichlet condition that the $E = E_{1D}$ along the model edges, where $E_{1D}(z)$ is the electric field computed for the 1D conductivity model derived the vertical column of cells along each side of the model. As Bob has pointed out in his notes, rigorous boundary conditions for the top of the model exist yet are difficult to implement. Thus along the top and bottom it is common practice to apply either a linear of cosine taper between the 1D fields computed for the left and right side 1D models. Also, the model grid usually includes tens of kilometers of air so any error introduced by this boundary condition is negligible within the Earth. To implement the boundary conditions, consider a ring of fictitious nodes surrounding the true model grid where the value of E_{1D} is known for each fictitious node. Now consider the 2D stencil (equation 25) for a true grid boundary node. For example, along the left boundary, the term $E_{i-1,j}$ corresponds to a fictitious node. We set $E_{i-1,j} = E_{1D}(z)$ and then move this term to the right side of the equation. We follow the same approach for the right boundary and the top and bottom. Thus the vector $\mathbf{b}$ will mostly be 0, but will have values $-E_{1D}(z)$ for nodes along the model boundary.

One final consideration for computing MT responses is the computation of the auxiliary magnetic field for the TE mode. From Faraday's law we have

$$H_y = \frac{-i}{\omega\mu_0}\frac{\partial E_x}{\partial z}. \tag{27}$$

You might be tempted to take a centered difference to compute $\frac{\partial E_x}{\partial z}$ since it is accurate to $O(h^2)$. However, MT sites are usually located along the conductivity boundary between air and land (or sea and seafloor) and so the vertical derivative of E can change across the boundary. It is common practice to compute derivatives by first

fitting a parabola to the field values at the 3 nodes that lie on and below the air-earth contact, then analytically evaluating the derivative of the parabola at z=0 to get $\frac{\partial E_x}{\partial z}$. A similar 2D FD formulation can be made for the TM mode, but special care needs to be taken for the $\nabla \cdot \frac{1}{\sigma} \nabla$ operator (see for example, Brewitt-Taylor and Weaver, 1976).

3D Finite Difference Method

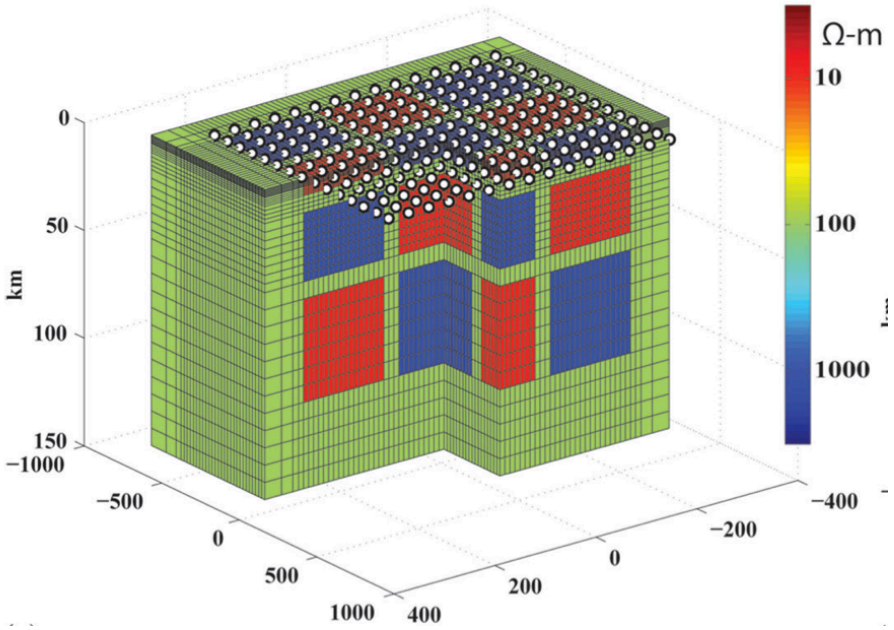

Figure 4: Example of a 3D model grid. From Egbert and Kelbert (2012).

Figure 4 shows an example 3D model grid (only the central portion is shown). In our 2D TE mode formulation, the scalar electric field is tangential to conductivity boundaries regardless of whether the field is on or off a node and thus the solution is guaranteed to obey the continuity of tangential field components. In 3D, we need to be careful where we evaluate the electric field vectors since conductivity contrasts can exists in any arbitrary location along x, y, and z. If we used a nodal basis to represent the field vectors where each node is surrounded by 8 conductivity cells, the solution could violate the boundary condition that the current normal to a boundary is continuous if the cell conductivities vary there. The commonly used solution to this

problem is the Yee staggered grid (Yee, 1966), where the field values are evaluated as components tangential to the cell edges, as shown in Figure 5. Thus, the continuity condition of tangential fields is explicitly enforced.

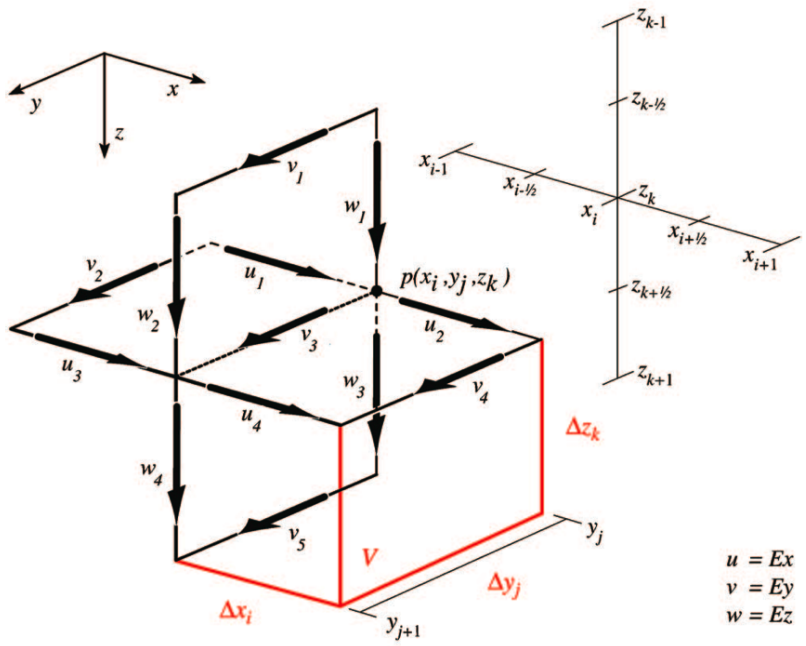

Figure 5: The basic 13 point paddle wheel stencil for a 3D staggered grid. The cell volume V contains a constant conductivity. Field values are evaluated along the edges of the conductivity cell. This paddle wheel corresponds to the 13 components needed to evaluate the curl-curl operator for the field vector at v_3, which is pointing in the y direction. Similar paddle wheels can be made for the x and z components. Figure from Weiss and Constable (2006).

Let's consider the curl-curl equation for the electric field:

$$\nabla \times \nabla \times \mathbf{E} + i\omega\mu_0\sigma\mathbf{E} = -i\omega\mu_0\mathbf{J}_s. \tag{28}$$

We do not have time to derive nor state the full FD solution to this equation, but interested readers can find it in Appendix A of Newman and Alumbaugh (1995). The curl-curl operator is evaluated using centered differences of the field values along the

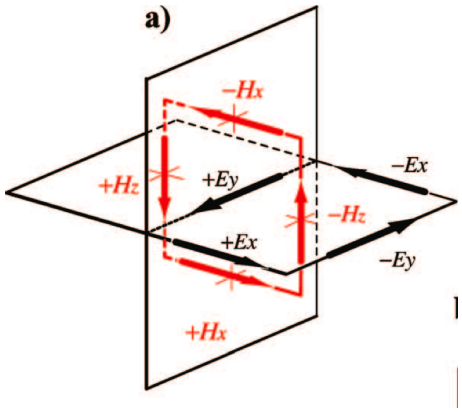

Figure 6: Circulation of the electric field vectors along on flap of the paddle wheel is used to approximate the magnetic field in the center of the flap. Similarly, the circulation of the magnetic field from the four flaps is used to estimate the electric field along the axis of the paddle wheel. Figure from Weiss and Constable (2006).

edges of the finite difference paddle wheel. An example of the paddle wheel for a y component is shown in Figure 5. If should be easy to see in Figure 6 that circulation of the electric field vectors along one flap of the paddle wheel is used to approximate the magnetic field in the center of the flap via Faraday's Law. Similarly, the circulation of the magnetic field from the four flaps is used to estimate the electric field along the axis of the paddle wheel (via Ampere's Law). As in the 2D case, the value for the conductivity in equation 28 is a volume weighted average of the 4 conductivities of cells surrounding a given field vector. Boundary conditions for controlled-source EM problems are usually set to the homogeneous Dirichlet condition ($\mathbf{E} = 0$ on the outer boundary). For 3D MT, the boundary values are set to be the fields from a 2D model from each side of the 3D model, where two parallel sides require 2D TE mode calculation sand the other two sides required 2D TM mode calculations. While that is ideal, many 3D codes simply use 1D calculations for the model boundary values. For those seeking a gratuitous complex derivation, the full 3D FD formulation that includes general anisotropic conductivity tensor is given in Weiss and Newman (2003).

3D Finite Volume Method

A method that is similar to finite differences is the finite *volume* (FV) method. Instead of the outright numerical differences used by the FD approximate the differential equation, the problem is recast into the integral form and the integrals are evaluated over small control volumes (equivalent to the FD cells). Weiss and Constable (2006) is a recent example where the FV method is used to model the marine controlled-source EM problem in 3D. First, the entire modeling domain is discretized into small volumes Ω with boundary Γ. Then equation 28 is integrated over each volume, shown as

$$\int_{\Omega} \nabla \times \nabla \times \mathbf{E} \, d\Omega + \int_{\Omega} i\omega\mu_0\sigma\mathbf{E} \, d\Omega = -\int_{\Omega} i\omega\mu_0\mathbf{J}_s \, d\Omega. \tag{29}$$

Using the identity

$$\int_{\Omega} \nabla \times \mathbf{A} \, d\Omega = \int_{\Gamma} \mathbf{n} \times \mathbf{A} \, d\Gamma, \tag{30}$$

the left most term in equation 29 is re-written into a surface integral over each volume, giving

$$\int_{\Gamma} \mathbf{n} \times \nabla \times \mathbf{E} \, d\Gamma + \int_{\Omega} i\omega\mu_0\sigma\mathbf{E} \, d\Omega = -\int_{\Omega} i\omega\mu_0\mathbf{J}_s \, d\Omega. \tag{31}$$

The integrals in this equation are then approximated by defining electric field vectors along the edges of the volume in an analogous manner to the 3D FD method. The derivatives inside the surface integral are approximated using finite differences. In fact, the resulting coefficient matrix for the left hand side integrals is exactly the same as the FD formulation. An advantage of using the FV formulation lies in the flexibility of the integral formulation of the right hand side, which permits higher order integration techniques if necessary. For instance, in regions where the primary field has singularities, higher order integration techniques can sometimes improve accuracy as shown in (Weiss and Constable, 2006). Let's consider a simple case of a point dipole where $\mathbf{J}_s = \mathbf{p}\,\delta(\mathbf{r} - \mathbf{r}_0)$ where the vector $\mathbf{p}$ describes the dipole magnitude and direction The right hand side is then simply

$$-\int_{\Omega} i\omega\mu_0\mathbf{J}_s \, d\Omega = -\int_{\Omega} i\omega\mu_0\mathbf{p}\,\delta(\mathbf{r} - \mathbf{r}_0) \, d\Omega = -i\omega\mu_0\mathbf{p}. \tag{32}$$

The Finite Element Method

The finite element (FE) method offers much more flexibility than the FD method since FE grids can be composed of irregular triangular and tetrahedral elements, which are ideal for modeling arbitrarily complex structures. Figure 7 shows an example 2D FE model that can be created easily with finite element Delaunay triangulation routines. Creating such a model with the stair-step approximation used with FD grids can be time consuming and also require dense gridding to accurately capture the various sloping features.

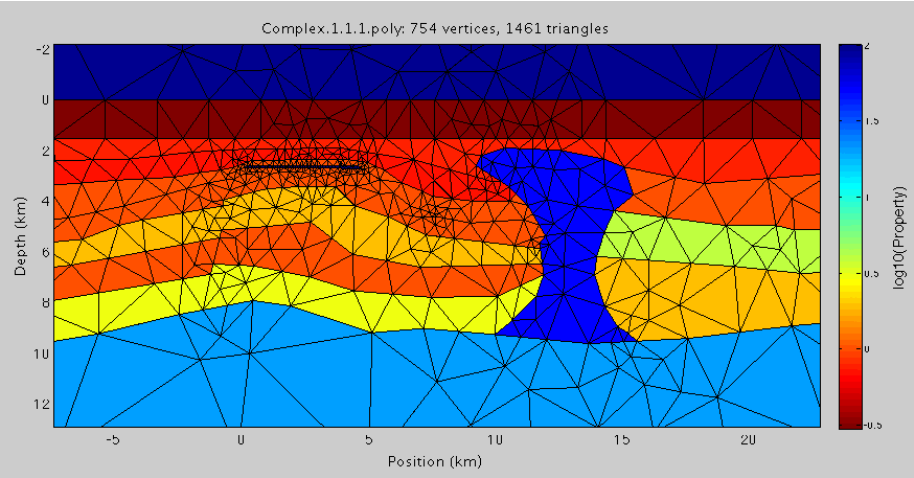

Figure 7: Example finite element model consisting of unstructured triangular elements.

2D Finite Element Method

We start with the 2D TE mode equation for the total field

$$-\nabla^2 E + i\omega\mu\sigma E = 0. \tag{33}$$

The first step in the FE method is to recast this strong form of the partial differential equation into the weak form. This is done by multiplying equation 33 by a test function v and integrating over the domain $\Omega \subset \mathbb{R}^2$:

$$-\int_\Omega \nabla^2 E\, v\, d\Omega + i\int_\Omega \omega\mu\sigma E\, v\, d\Omega = 0. \tag{34}$$

Using the formula for integration by parts

$$v\nabla \cdot \nabla u = \nabla \cdot (v\nabla u) - \nabla v \cdot \nabla u, \tag{35}$$

we can write equation 34 as

$$\int_\Omega \nabla v \cdot \nabla E \; d\Omega - \int_\Omega \nabla \cdot (v\nabla E) \; d\Omega + i \int_\Omega v\omega\mu\sigma E \; d\Omega = 0. \tag{36}$$

Next, we apply the divergence theorem to the second term on the left hand side,

$$\int_\Omega \nabla \cdot (v\nabla E) \; d\Omega = \int_\Gamma v \frac{\partial E}{\partial n} \; d\Gamma, \tag{37}$$

where Γ is the union of the interior and exterior boundaries of Ω. On interior boundaries this integral vanishes since we integrate in opposite directions on each side of the boundary. By specifying that v vanishes on the exterior boundary, we then have

$$\int_\Omega \nabla v \cdot \nabla E \; d\Omega + i \int_\Omega v\omega\mu\sigma E \; d\Omega = 0. \tag{38}$$

Alas we have mapped the original second order problem into a first order differential equation, but at the cost of restricting it's solution to the space of v.

For the finite element method, we divide up the domain Ω into m finite elements defined by n nodes. Here we will use unstructured triangular finite elements, as shown in Figure 7. Within each element the conductivity is constant σ_e. For the test functions we use special functions v_i that have value 1 at node i and are zero at all other nodes. Along edges connecting node i to another node j, the basis functions can be defined to have linear, quadric, cubic, etc shape. Here we will use linear basis functions. So you can think of the basis functions as tent functions with value 1 at node i that fall off linearly to 0 at the other surrounding nodes. Next we invoke Galerkin's method, which is to define the electric field using the same test functions v_j as a basis, written as

$$E(y, z) = \sum_{j=1}^{n} E_j v_j, \tag{39}$$

where E_j is the value of the electric field at node j. Since the functions v_j are linear, we can say that we have expanded E in terms of a linear basis. It's worth point out here that one advantage of the FE method is the ability to use higher order basis functions, if necessary. However, the higher order basis functions add complexity so here we will stick to a linear basis.

Now we can form a linear system used to solve for the nodal electric fields E_j. With the basis function expansion, we can write

$$\sum_{j=1}^{n} \int_{\Omega} (\nabla v_i \cdot \nabla v_j + i\omega\mu\sigma_e \, v_i \, v_j) E_j \, d\Omega = 0. \qquad i = 1, ..., n \tag{40}$$

Looking at the left hand side of this equation, it is evident that the integrals will be non-trivial only when i and j are nodes in the same element. Thus, we can think of the global integral as the sum of integrals over each element

$$\sum_{e=1}^{m} \sum_{j=1}^{n} \int_{\Omega_e} (\nabla v_i \cdot \nabla v_j + i\omega\mu\sigma_e \, v_i \, v_j) E_j \, d\Omega_e = 0, \qquad i = 1, ..., n \tag{41}$$

where Ω_e is the domain of element e. Thus we can build up the matrix for the linear system element by element in a straightforward fashion:

$$\mathbf{A}\mathbf{x} = \mathbf{b}, \tag{42}$$

where

$$\mathbf{A}_{ij} = \sum_{e=1}^{m} \int_{\Omega_e} (\nabla v_i \cdot \nabla v_j + i\omega\mu\sigma_e \, v_i \, v_j), \tag{43}$$

$$\mathbf{x}_j = E_j, \tag{44}$$

and

$$\mathbf{b}_j = 0. \tag{45}$$

For each element, the integral contribution of equation 43 results in a 3 x 3 local matrix that can be added into the global matrix at the correct i and j indices.

To finish up, let's look at how to compute the integral terms. First we need a more complete description of the basis functions v_i. Within a triangle with corner nodes at positions $(y_i, z_i, i = 1, 2, 3)$, we can write the linear basis function v_i associated with each node as

$$v_i = \frac{1}{2\triangle} \left(a_i + b_i y + c_i z \right), \tag{46}$$

where

$$a_i = y_j z_k - y_k z_j \quad b_i = z_j - z_k, \quad c_i = y_k - y_j, \tag{47}$$

i, j, k are cyclic permutations of 1,2,3 and $\triangle$ is the element area

$$\triangle = \frac{1}{2} \left(a_1 + x_1 b_1 + z_1 c_1 \right). \tag{48}$$

The linear v_i are also known as barycentric coordinates. The easiest method is to simply use Gauss quadrature since that is trivial to program and the order can be chosen to exactly integrate to the order of the polynomial basis functions v_i. Alternatively, the integrals can be evaluated analytically. For example, for the 3 nodes of an element, we can write

$$\int_{\Omega_e} \nabla v_i \cdot \nabla v_j \, d\Omega = \frac{1}{4\triangle} \begin{bmatrix} h_{11} & h_{12} & h_{13} \\ h_{12} & h_{22} & h_{23} \\ h_{13} & h_{23} & h_{33} \end{bmatrix} \tag{49}$$

where

$$h_{ij} = b_i b_j + c_i c_j. \tag{50}$$

Since the basis functions are polynomials, their integrals over a triangular element are evaluated exactly using the well known formula

$$\int_{\triangle} v_1^a v_2^b v_3^c \, d\triangle = \frac{2\triangle a! b! c!}{(a+b+c+2)!}. \tag{51}$$

Thus we have

$$\int_{\Omega_e} i\omega\mu\sigma_e \, v_i \, v_j \, d\Omega = i\omega\mu\sigma \, \frac{\triangle}{12} \begin{bmatrix} m_1 & m_2 & m_2 \\ m_2 & m_1 & m_2 \\ m_2 & m_2 & m_1 \end{bmatrix} \tag{52}$$

where

$$m_1 = 2, \quad m_2 = 1. \tag{53}$$

Notice that σ is constant over the element and hence the finite element method is free of the annoying conductivity averaging approximations needed by the finite difference method.

Lastly, we must implement some boundary conditions, which can be done with a similar approach to what we did for the FD method. We specify the nodes on the left and right sides to have values $E_{1D}(z)$ and a taper of these values along the top and bottom. There are a few ways that the boundary conditions can be incorporated into the linear system but we don't have time to review them here. The basic idea is to subtract the the boundary values present in the product $\mathbf{Ax}$ off of the right hand side vector $\mathbf{b}$.

The FE formulation for the TM mode is derived in a similar manner, but care needs to be taken in the boundary integral, which does not cancel out across conductivity contrasts.

Another advantage of finite elements is that it is relatively simple to refine the FE grid in regions where the solution accuracy is insufficient—this process is called adaptive refinement and is a rapidly evolving research topic in FE methods. For examples of adaptive refinement applied to marine MT and CSEM, see (Key and Weiss, 2006; Li and Key, 2007; Key and Ovall, 2011).

3D Finite Element Method

Like the 3D FD method, care needs to be taken when moving to 3D finite elements. It is common to use tetrahedral vector *edge* elements, where the degrees of freedom for the element are the 6 electric field values along the edges of a tetrahedral element (Figure 8). Thus, tangential electric field continuity is maintained across elements. Figure 9 shows some example tetrahedral meshes.

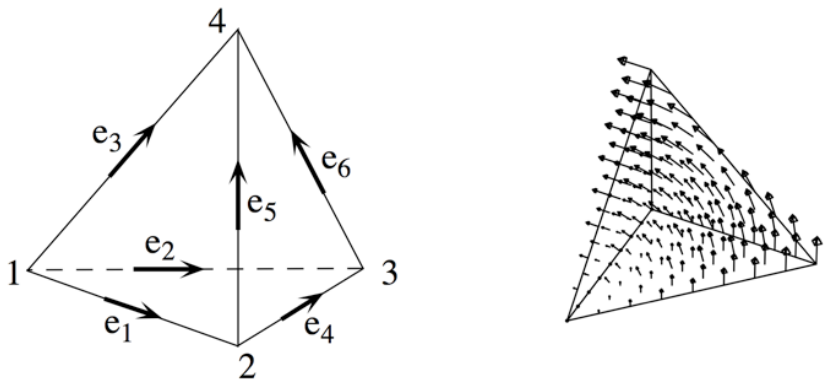

Figure 8: Tetrahedral edge element (left) and an example of the linear vector basis function associated with the upper-right edge (right).

Here we will consider a controlled-source EM problem where the sources are inside the model domain and the fields drop to infinitesimally small values at far distances. We can therefore impose the following boundary condition on the model domain Ω

$$\begin{cases} \hat{n} \times \mathbf{H} = 0 \ \text{ on } \Gamma_{\mathrm{N}}, \\ \hat{n} \times \mathbf{E} = 0 \ \text{ on } \Gamma_{\mathrm{D}}, \end{cases} \tag{54}$$

where Γ_N is the portion of the boundary where Neumann conditions are applied and Γ_D the portion of the boundary where Dirichelet conditions are applied. where Γ is

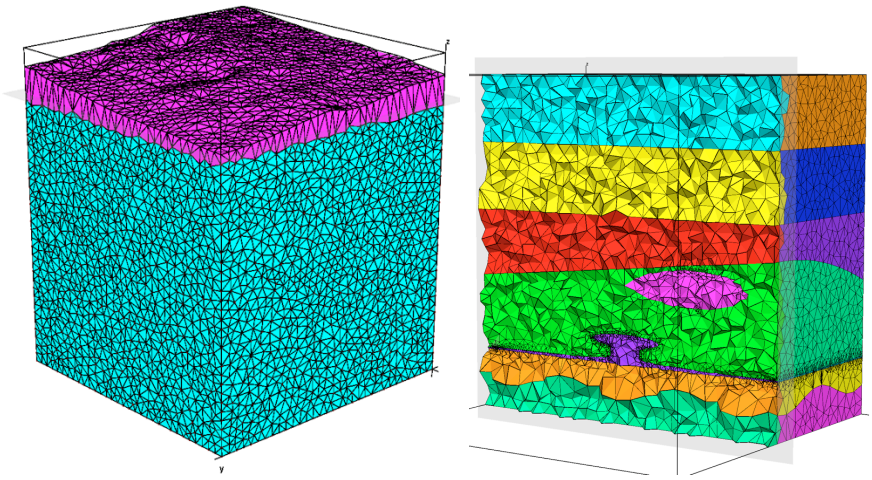

Figure 9: Example of tetrahedral meshes for a complex topography surface (left) and for multiple embedded structures (right).

the boundary of Ω. The weak statement of equation 6 is found by taking the dot product with a vector test function $\mathbf{v}$ and integrating over the domain:

$$\int_\Omega \mathbf{v} \cdot \nabla \times \nabla \times \mathbf{E}\, d\Omega + \int_\Omega \mathbf{v} \cdot i\omega\mu_0\sigma\mathbf{E}\, d\Omega = -\int_\Omega \mathbf{v} \cdot i\omega\mu_0\mathbf{J}_s\, d\Omega, \tag{55}$$

Applying the Green's theorem

$$\int_\Omega \mathbf{A} \cdot \nabla \times \nabla \times \mathbf{B}\, d\Omega = \int_\Omega \nabla \times \mathbf{A} \cdot \nabla \times \mathbf{B}\, d\Omega - \int_\Gamma \hat{n} \cdot (\mathbf{A} \times \nabla \times \mathbf{B})\, d\Gamma \tag{56}$$

to equation 55 yields

$$\begin{aligned} &\int_\Omega \nabla \times \mathbf{v} \cdot \nabla \times \mathbf{E}\, d\Omega + \int_\Omega \mathbf{v} \cdot i\omega\mu_0\sigma\mathbf{E}\, d\Omega = \\ &-i\omega\mu_0 \int_\Omega \mathbf{v} \cdot \mathbf{J}_s\, d\Omega + \int_\Gamma \hat{n} \cdot (\mathbf{v} \times \nabla \times \mathbf{E})\, d\Gamma. \end{aligned} \tag{57}$$

Using the vector identity

$$\mathbf{A} \cdot (\mathbf{B} \times \mathbf{C}) = -\mathbf{B} \cdot (\mathbf{A} \times \mathbf{C}) \tag{58}$$

the boundary integral in equation 57 is expanded as

$$\begin{aligned} \int_\Gamma \hat{n} \cdot (\mathbf{v} \times \nabla \times \mathbf{E})\, d\Gamma &= -\int_\Gamma \mathbf{v} \cdot (\hat{n} \times \nabla \times \mathbf{E})\, d\Gamma \\ = -\int_{\Gamma_D} \mathbf{v} \cdot (\hat{n} \times \nabla \times \mathbf{E})\, d\Gamma_D &+ i\omega\mu_0 \int_{\Gamma_N} \mathbf{v} \cdot (\hat{n} \times \mathbf{H})\, d\Gamma_N. \end{aligned} \tag{59}$$

Applying the boundary conditions defined in equation 54 to equation 57 yields

$$\int_{\Omega} \nabla \times \mathbf{v} \cdot \nabla \times \mathbf{E}\, d\Omega + \int_{\Omega} \mathbf{v} \cdot i\omega\mu_0\sigma\mathbf{E}\, d\Omega = -i\omega\mu_0 \int_{\Omega} \mathbf{v} \cdot \mathbf{J}_s\, d\Omega \tag{60}$$

Linear tetrahedral edge elements are described by a *vector* basis function for each edge that has a value of one on edge e and is zero on all other edges. A vector field $\mathbf{E}$ within an element is described as

$$\mathbf{E} = \sum_{e=1}^{6} E_e \mathbf{N}_e, \tag{61}$$

where E_e is the value of the field along edge e and $\mathbf{N_e}$ is the vector basis function for edge e. Since there are six edges per element, there are six degrees of freedom associated with each element. For an element with edge e connecting vertices i and j, the basis function is given by

$$\mathbf{N}_e = \lambda_i \nabla\lambda_j - \lambda_j \nabla\lambda_i, \tag{62}$$

where λ_i is the barycentric (or volume) coordinate for node i. λ_i has a value of one at node i and is zero at all other nodes.

The barycentric coordinates for tetrahedron t have the form

$$\lambda_i = \frac{1}{6V_t}(a_i + b_i x + c_i y + d_i z). \tag{63}$$

For a given point (x, y, z) inside tetrahedron t, the following linear system of equations can be used to get the corresponding volume coordinates

$$\begin{bmatrix} \lambda_1 \\ \lambda_2 \\ \lambda_3 \\ \lambda_4 \end{bmatrix} = \frac{1}{6V_t} \begin{bmatrix} a_1 & b_1 & c_1 & d_1 \\ a_2 & b_2 & c_2 & d_2 \\ a_3 & b_3 & c_3 & d_3 \\ a_4 & b_4 & c_4 & d_4 \end{bmatrix} \begin{bmatrix} 1 \\ x \\ y \\ z \end{bmatrix}. \tag{64}$$

Since the volume coordinates have a value of one at their respective vertices and are zero at the other three nodes, for tetrahedron t with vertices $(x_i, y_i, z_i, i = 1...4)$, we can write out the following linear system of equations to find the value of the coefficients a_i, b_i, c_i, and d_i as

$$\begin{bmatrix} 1 & 0 & 0 & 0 \\ 0 & 1 & 0 & 0 \\ 0 & 0 & 1 & 0 \\ 0 & 0 & 0 & 1 \end{bmatrix} = \frac{1}{6V_t} \begin{bmatrix} a_1 & b_1 & c_1 & d_1 \\ a_2 & b_2 & c_2 & d_2 \\ a_3 & b_3 & c_3 & d_3 \\ a_4 & b_4 & c_4 & d_4 \end{bmatrix} \begin{bmatrix} 1 & 1 & 1 & 1 \\ x_1 & x_2 & x_3 & x_4 \\ y_1 & y_2 & y_3 & y_4 \\ z_1 & z_2 & z_3 & d_4 \end{bmatrix} \tag{65}$$

This leads to the following formulas for computing the coefficients

$$\begin{aligned} a_i &= (\, x_j\,(y_k z_l - y_l z_k) + x_k(y_l z_j - y_j z_l) + x_l(y_j z_k - y_k z_j)\,)\,\delta_i, && (66)\\ b_i &= (\, y_j\,(z_l - z_k) + y_k(z_j - z_l) + y_l(z_k - z_j)\,)\,\delta_i, && (67)\\ c_i &= (\, z_j\,(x_l - x_k) + z_k(x_j - x_l) + z_l(x_k - x_j)\,)\,\delta_i, && (68)\\ d_i &= (\, x_j\,(y_l - y_k) + x_k(y_j - y_l) + x_l(y_k - y_j)\,)\,\delta_i, && (69) \end{aligned}$$

where subscripts i, j, k, l should be cyclically permuted between 1,2,3,4 and δ_i is a sign operator defined as

$$\delta_i = \begin{cases} +1 & i = 1, 3 \\ -1 & i = 2, 4 \end{cases} . \qquad (70)$$

A few interesting relations for the coefficients are

$$\sum_i^4 a_i = 6V_t, \qquad (71)$$

and

$$\sum_i^4 b_i = \sum_i^4 c_i = \sum_i^4 d_i = 0. \qquad (72)$$

The gradient terms in the basis function given in equation 62 can each be written as

$$\nabla\lambda_i = \frac{1}{6V_t} \begin{bmatrix} b_i \\ c_i \\ d_i \end{bmatrix} . \qquad (73)$$

The full basis function for edge e connecting nodes i and j is then

$$\mathbf{N}_e = \lambda_i \nabla\lambda_j - \lambda_j \nabla\lambda_i = \frac{1}{6V_t}(a_i + b_i x + c_i y + d_i z)\frac{1}{6V_t} \begin{bmatrix} b_j \\ c_j \\ d_j \end{bmatrix} - \frac{1}{6V_t}(a_j + b_j x + c_j y + d_j z)\frac{1}{6V_t} \begin{bmatrix} b_i \\ c_i \\ d_i \end{bmatrix} . \qquad (74)$$

This simplifies to

$$\mathbf{N}_e = \frac{1}{36\,V_t^2} \begin{bmatrix} \alpha_1 + \alpha_2 y + \alpha_3 z \\ \alpha_4 - \alpha_2 x + \alpha_5 z \\ \alpha_6 - \alpha_3 x - \alpha_5 y \end{bmatrix} \qquad (75)$$

where

$$\begin{aligned} &\alpha_1 = a_i b_j - a_j b_i\,, \quad \alpha_2 = c_i b_j - c_j b_i\,, \quad \alpha_3 = d_i b_j - d_j b_i\,, \\ &\alpha_4 = a_i c_j - a_j c_i\,, \quad \alpha_5 = d_i c_j - d_j c_i\,, \quad \alpha_6 = a_i d_j - a_j d_i\,. \end{aligned} \qquad (76)$$

It is now obvious that the basis functions are divergence free ($\nabla \cdot \mathbf{N_e} = 0$) since the derivatives are zero for each component (for example, since, for example, the x component depends only on y and z, not x and hence).

The formation of the finite element system of equations follows the same approach as shown earlier for the 2D MT FE problem.

References

Brewitt-Taylor, C. R., and J. T. Weaver, 1976, Finite-difference solution of 2-dimensional induction problems: Geophysical Journal Of The Royal Astronomical Society, **47**, 375–396.

Egbert, G. D., and A. Kelbert, 2012, Computational recipes for electromagnetic inverse problems: Geophysical Journal International, **189**, 251–267.

Key, K., and J. Ovall, 2011, A parallel goal-oriented adaptive finite element method for 2.5-D electromagnetic modelling: Geophysical Journal International, **186**, 137–154.

Key, K., and C. Weiss, 2006, Adaptive finite element modeling using unstructured grids: the 2D magnetotelluric example: Geophysics, **71**, G291–G299.

Li, Y., and K. Key, 2007, 2D marine controlled-source electromagnetic modeling: Part 1–An adaptive finite element algorithm: Geophysics, **72**, WA51–WA62.

Newman, G. A., and D. L. Alumbaugh, 1995, Frequency-domain modelling of airborne electromagnetic responses using staggered finite differences: Geophysical Prospecting, **43**, 1021–1042.

Weiss, C. J., and S. Constable, 2006, Mapping Thin Resistors in the Marine Environment, Part II: Modeling and Analysis in 3D: Geophysics, **71**, G321–G332.

Weiss, C. J., and G. A. Newman, 2003, Electromagnetic induction in a generalized 3D anisotropic earth, Part 2: The LIN preconditioner: Geophysics, **68**, 922–930.

Yee, K. S., 1966, Numerical Solution Of Initial Boundary Value Problems Involving Maxwells Equations In Isotropic Media: IEEE Transactions On Antennas And Propagation, **AP14**, 302–307.